CHAPTER 4

ANALYSIS OF AZIMUTHAL PARTITION PERIODIC DISC LOADED COAXIAL STRUCTURE FOR BI-FREQUENCY MILO USING EQUIVALENT CIRCUIT APPROACH*

*Part of this work has been published as:

Arjun Kumar, Prabhakar Tripathi, Smrity Dwivedi, and Pradip Kumar Jain, "Analysis of Azimuthal Partition Periodic Disc Loaded Coaxial Structure for Bi-Frequency MILO using Equivalent Circuit Approach," *IEEE Transaction on Plasma Science*, vol. 48, no. 9, pp. 3030-3039, 2020.

4.1. Overview

In this Chapter, an equivalent circuit approach has been used to study the bi-frequency generation by the azimuthally partitioned axially periodic metal disc loaded coaxial structure. The equivalent circuit approach used in this chapter eliminates all the limitation which was used previously and explained in chapter 2. Such as, Dixit and Jain (2016) had limited their equivalent circuit analysis for azimuthally symmetric structures and for only symmetric TM_{0n} modes and unable to perform the complete analysis (i.e. like symmetric TE mode and asymmetric modes supported by the structure) of coaxial structure. Here, in the present approach the effect of all harmonics present within the structure are considered and the expression of the equivalent series inductance per unit length and equivalent shunt capacitance per unit length has been obtained for the equivalent transmission line. In addition, with the help of computed equivalent series induction and equivalent shunt capacitance, expressions for the dispersion relation, phase velocity, and characteristic impedance have been obtained. In order to validate the numerical analysis, the structure has been firstly simulated with the help of CST microwave studio and then the analytically obtained results (such as dispersion behavior and phase velocity) have been compared with the results obtained from simulation. The comparison of results shows that the relative error is below 5%, which shows a good agreement between them.

4.2. Introduction

In recent years, multi-frequency high power microwave (HPM) sources became popular due to their potential application in the field of plasma heating, defense application, and

linear particle accelerator [Benford *et al.* (2007)]. Different HPM sources, like relativistic backward wave oscillator (RBWO), magnetically insulated line oscillator (MILO), and transit time oscillator (TTO) have been developed to generate bi-frequency RF [Tang *et al.* (2012), Wang *et al.* (2010) and He *et al.* (2011)]. These sources can generate RF power in two/or more frequencies either in dual-band or single-band. The device which generates RF power at two different frequencies belonging to a different frequency band is called a dual-band device. Generally, the dual-band devices are the combination of two different/same device which operate in a different band in a single device structure such as MILO and MILO, MILO and Vircator, MILO and coaxial TTO [Ju *et al.* (2014), Zhang *et al.* (2015) and Xiao *et al.* (2009)]. In single-band bi-frequency devices; the device generates RF power at two different frequencies belonging to a single-band. The bi-frequency single-band device can be designed in two ways: (*a*) by azimuthally varying the interaction structure [Wang *et al.* (2010)], or (*b*) by axially varying the interaction structure [Tang *et al.* (2012)]. A periodic metal disc loaded coaxial structure with azimuthally partitioned finds its application in generating two different and stable frequencies within a single high-power microwave (HPM) source.

Magnetically insulated line oscillator (MILO) is an attractive device to generate bi-frequency in GHz range with power in the GW level, due to its compact size and self-magnetic insulation mechanism [Lemke *et al.* (1997)]. The magnetic field developed in the structure due to the presence of the dense electrons beam, through the higher applied voltage which helps in the generation of stable bi-frequency. Since the structure has potential strategic applications, it is essential to analyze the electromagnetic (EM) behavior of azimuthally partitioned bi-frequency magnetically

insulated line oscillator (BFMILO). An equivalent circuit approach has been used here to study the EM behavior of the device. The generation of bi-frequency through a single device utilizes the concept of azimuthal partition of the structure. To analyze the axially periodic disc loaded coaxial structure; a dispersion relation is an excellent tool that provides information about the resonance frequency of the RF interaction structure and highlights the effect of various structural parameters on the structure dispersion behavior. In the past, many authors characterized the disc-loaded waveguiding structure using different methods, such as Wang *et al*. used a field matching technique to analyze the disc-loaded coaxial waveguide structure [Wang *et al.* (2007)]. Zhang *et al.* used the modified Rayleigh-Fourier method to analyze the periodic disc-loaded cylindrical waveguide structure with axial and azimuthal corrugations [Zhang *et al.* (2005)]. The equivalent circuit analysis for disc-loaded coaxial structure has been carried out for azimuthally symmetric TM_{0n} modes by Dixit *et al.* [Dixit and Jain (2016)]. Wang *et al.* used field matching theory to analyze the periodic disc loaded coaxial structure with azimuthal partition [Wang *et al.* (2010)]. The field matching technique involved higher-order matrices which is comparatively difficult to solve and takes a lot of computational time [Dwivedi and Jain (2012), (2012), and (2013)]. The equivalent circuit analysis is less involved and cumbersome compared with other techniques. To analyze the EM behavior of the structure, the equivalent circuit approach is used which is found much simpler to handle and yields equally accurate results that of the involved field analysis. Using this approach, we can also perform the impedance matching at the different sections of the device [Dixit and Jain (2016)].

The equivalent circuit analysis is performed to analyze the EM behavior of the azimuthally partitioned axially periodic discs loaded coaxial waveguide structure. The

EM field distributions generated inside this structure exhibit both axial and azimuthal harmonics therefore the individual TE or TM mode no longer satisfies the boundary conditions. Thereby the EM eigenmodes within the device are having all the six components of electric and magnetic fields resulting in hybrid modes (HEM modes) generation inside the structure.

In this chapter, the azimuthally partitioned periodic discs loaded coaxial structure analyzed using the equivalent circuit approach, and a study of its dispersion characteristics is performed in Section-4.3. In Section-4.4, the computed results obtained using the developed analysis and compared with those values obtained through EM simulation; for the validation of the developed analysis. Also, the effect of different structural parameters on its dispersion characteristics associated with the different modes is presented in this section. Finally, the conclusion of this study is presented in Section- 4.5.

4.3. Analysis

The equivalent circuit analysis is performed to characterize the azimuthally partitioned periodic metal disc loaded coaxial structure which is shown in Fig. 4.1. The geometry consists of an axially periodic metal disc with a thickness (*T*), cylindrical metal conductor at the center (i.e. used as the cathode) and the two half-cylindrical waveguides have different wall radius (i.e. one half of the cylinder continuous from $0^{o} \le \theta \le 180^{o}$ with wall radius (i.e. r_{w2}), while other from $180^{o} \le \theta \le 360^{o}$ with wall radius (i.e. r_{w1})). Fig. 4.1(a) and 4.1(b) shows the sectional and front view of the azimuthally partitioned axially periodic disc loaded coaxial structure, respectively. The parameters associated with the structure are: r_c, r_d, r_{w1}, r_{w2}, L, and T represents the

cathode radius, inner disc radius, wall radius of azimuthal section-1, wall radius of azimuthal section-2, periodicity, and thickness of the disc, respectively. According to Floquet's theorem, the unit cell of the structure is enough to analyze the EM behavior of the infinite periodic structure. The azimuthally partitioned axially periodic metal disc loaded coaxial structure is divided into three regions i.e. region-*I* (i.e. between the cathode to the tip of the metal disc, $r_c \le r \le r_d$), region-*II* (between the tip of the metal disc to wall radius, $r_d \le r \le r_{w1}$, $180^\circ \le \theta \le 360^\circ$) and region-*III* ($r_{w1} \le r \le r_{w2}$, $0^\circ \le \theta \le 180^\circ$). The superscript *I*, *II*, and *III* associated with the different parameter indicates that the parameter belongs to the regions *I*, *II*, and *III*, respectively.

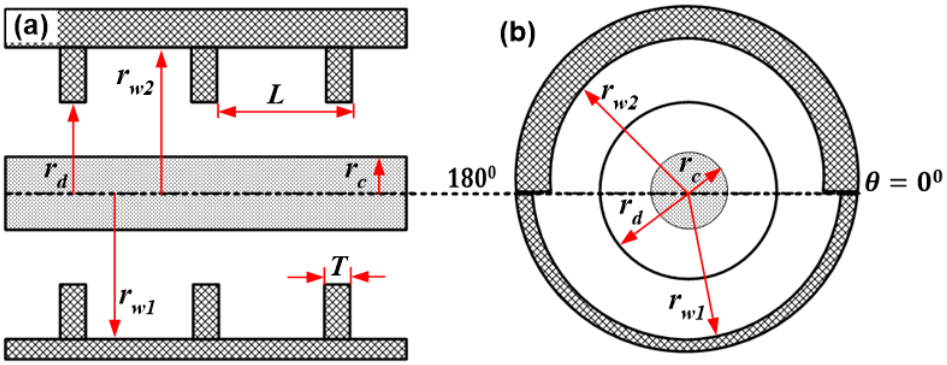

Figure 4.1: Schematic of an azimuthally partitioned axially periodic metal disc loaded coaxial structure: (a) sectional view (b) front view.

It is assumed that the region-*I* of the structure supports the traveling waves while the region-*II* and region-*III* support the standing waves. In order to obtain the field components in the different regions *I*, *II*, *III* of the structure, it is assumed that the EM fields are time-independent, the space harmonics of the traveling wave are due to the axial periodicity of the structure, and the modal harmonics of the standing wave present in the regions-*II* and *III* are due to the reflections of EM waves from the metallic

surfaces. Since the structure is azimuthally partitioned, therefore the pure TE or TM mode does not exist in the structure. In place of symmetrical TE and TM modes, the structure supports the asymmetrical modes (i.e. HEM mode). Since the structure is periodic in the axial (*z*) direction as well as periodic in the azimuthal (θ) direction. The field components in the different regions of the structure in the cylindrical coordinate system (r,θ,z) can be expressed as [Wang *et al.* (2010) and Singh *et al.* (2004)]:

(i). Region *I* (i.e. $r_c \le r \le r_d$)

$$E_r^I = \sum_{\upsilon=-\infty}^{\infty}\sum_{n=-\infty}^{\infty}\left[-i\beta_n^I\gamma_n^I U'_{\upsilon,n}(r)A_{\upsilon,n}^I - \frac{\upsilon\omega\mu}{r}V_{\upsilon,n}(r)B_{\upsilon,n}^I\right]\times\exp(-i\beta_n^I z)\exp(-i\upsilon\theta) \tag{4.1}$$

$$E_\theta^I = \sum_{\upsilon=-\infty}^{\infty}\sum_{n=-\infty}^{\infty}\left[-\frac{\upsilon\beta_n^I}{r}U_{\upsilon,n}(r)A_{\upsilon,n}^I + i\omega\mu\gamma_n^I V'_{\upsilon,n}(r)B_{\upsilon,n}^I\right]\times\exp(-i\beta_n^I z)\exp(-i\upsilon\theta) \tag{4.2}$$

$$E_z^I = \sum_{\upsilon=-\infty}^{\infty}\sum_{n=-\infty}^{\infty}(k^2-(\beta_n^I)^2)U_{\upsilon,n}(r)A_{\upsilon,n}^I\times\exp(-i(\beta_n^I z+\upsilon\theta)) \tag{4.3}$$

$$H_r^I = \sum_{\upsilon=-\infty}^{\infty}\sum_{n=-\infty}^{\infty}\left[-i\beta_n^I\gamma_n^I V'_{\upsilon,n}(r)B_{\upsilon,n}^I + \frac{\upsilon\omega\varepsilon}{r}U_{\upsilon,n}(r)A_{\upsilon,n}^I\right]\times\exp(-i\beta_n^I z)\exp(-i\upsilon\theta) \tag{4.4}$$

$$H_\theta^I = \sum_{\upsilon=-\infty}^{\infty}\sum_{n=-\infty}^{\infty}\left[-\frac{\upsilon\beta_n^I}{r}V_{\upsilon,n}(r)B_{\upsilon,n}^I - i\omega\varepsilon\gamma_n^I U'_{\upsilon,n}(r)A_{\upsilon,n}^I\right]\times\exp(-i\beta_n^I z)\exp(-i\upsilon\theta) \tag{4.5}$$

$$H_z^I = \sum_{\upsilon=-\infty}^{\infty}\sum_{n=-\infty}^{\infty}(k^2-(\beta_n^I)^2)V_{\upsilon,n}(r)B_{\upsilon,n}^I\times\exp(-i(\beta_n^I z+\upsilon\theta)) \tag{4.6}$$

here, $\beta_n^I = \beta_0^I + 2n\pi/L$ is the axial propagation constant; γ_n^I $((\gamma_n^I)^2 = k^2-(\beta_n^I)^2)$ is the radial propagation constant, $n = 0,\pm1,\pm2,\pm3,...$, $\upsilon = 0,\pm1,\pm2,\pm3,...$; $A_{\upsilon,n}^I$, $B_{\upsilon,n}^I$ is the undetermined coefficient; $U_{\upsilon,n}(r)$, $V_{\upsilon,n}(r)$, $U'_{\upsilon,n}(r)$, $V'_{\upsilon,n}(r)$ are represented as the Bessel function. The prime sign indicates the differentiation of that parameter with respect to *r*.

$$U_{\upsilon,n}(r) = Y_\upsilon(\gamma_n^I r_c)J_\upsilon(\gamma_n^I r) - J_\upsilon(\gamma_n^I r_c)Y_\upsilon(\gamma_n^I r) \tag{4.7}$$

$$V_{\upsilon,n}(r) = Y'_\upsilon(\gamma_n^I r_c)J_\upsilon(\gamma_n^I r) - J'_\upsilon(\gamma_n^I r_c)Y_\upsilon(\gamma_n^I r) \tag{4.8}$$

$$U'_{\upsilon,n}(r) = Y_\upsilon(\gamma_n^I r_c)J'_\upsilon(\gamma_n^I r) - J_\upsilon(\gamma_n^I r_c)Y'_\upsilon(\gamma_n^I r) \tag{4.9}$$

$$V'_{\upsilon,n}(r) = Y'_\upsilon(\gamma_n^I r_c)J'_\upsilon(\gamma_n^I r) - J'_\upsilon(\gamma_n^I r_c)Y'_\upsilon(\gamma_n^I r) \quad . \tag{4.10}$$

(ii). Region *II* (i.e. $r_d \le r \le r_{w1}$)

$$\begin{aligned} E_r^{II} = \sum_{\upsilon=-\infty}^{\infty}\sum_{m=1}^{\infty}\{&-\beta_m^{II}\gamma_m^{II}[J'_\upsilon(\gamma_m^{II}r)A_{\upsilon,m}^{II} + Y'_\upsilon(\gamma_m^{II}r)B_{\upsilon,m}^{II}] \\ &-\frac{\upsilon\omega\mu}{r}[J_\upsilon(\gamma_m^{II}r)C_{\upsilon,m}^{II} + Y_\upsilon(\gamma_m^{II}r)D_{\upsilon,m}^{II}]\}\cos(\beta_m^{II}z)\times\exp(-i\upsilon\theta) \end{aligned} \tag{4.11}$$

$$\begin{aligned} E_\theta^{II} = \sum_{\upsilon=-\infty}^{\infty}\sum_{m=1}^{\infty}\{&\frac{i\upsilon\beta_m^{II}}{r}\left[J_\upsilon(\gamma_m^{II}r)A_{\upsilon,m}^{II} + Y_\upsilon(\gamma_m^{II}r)B_{\upsilon,m}^{II}\right] \\ &+i\omega\mu\gamma_m^{II}\left[J'_\upsilon(\gamma_m^{II}r)C_{\upsilon,m}^{II} + Y'_\upsilon(\gamma_m^{II}r)D_{\upsilon,m}^{II}\right]\}\cos(\beta_m^{II}z)\times\exp(-i\upsilon\theta) \end{aligned} \tag{4.12}$$

$$E_z^{II} = \sum_{\upsilon=-\infty}^{\infty}\sum_{m=1}^{\infty}(k^2-(\beta_m^{II})^2)[J_\upsilon(\gamma_m^{II}r)A_{\upsilon,m}^{II} + Y_\upsilon(\gamma_m^{II}r)B_{\upsilon,m}^{II}]\times\sin(\beta_m^{II}z)\exp(-i\upsilon\theta) \tag{4.13}$$

$$\begin{aligned} H_r^{II} = \sum_{\upsilon=-\infty}^{\infty}\sum_{m=1}^{\infty}\{&\beta_m^{II}\gamma_m^{II}\left[J'_\upsilon(\gamma_m^{II}r)C_{\upsilon,m}^{II} + Y'_\upsilon(\gamma_m^{II}r)D_{\upsilon,m}^{II}\right] \\ &+\frac{\upsilon\omega\varepsilon}{r}\left[J_\upsilon(\gamma_m^{II}r)A_{\upsilon,m}^{II} + Y_\upsilon(\gamma_m^{II}r)B_{\upsilon,m}^{II}\right]\}\sin(\beta_m^{II}z)\exp(-i\upsilon\theta) \end{aligned} \tag{4.14}$$

$$\begin{aligned} H_\theta^{II} = \sum_{\upsilon=-\infty}^{\infty}\sum_{m=1}^{\infty}\{&\frac{-i\upsilon\beta_m^{II}}{r}\left[J_\upsilon(\gamma_m^{II}r)C_{\upsilon,m}^{II} + Y_\upsilon(\gamma_m^{II}r)D_{\upsilon,m}^{II}\right] \\ &-i\omega\varepsilon\gamma_m^{II}\left[J'_\upsilon(\gamma_m^{II}r)A_{\upsilon,m}^{II} + Y'_\upsilon(\gamma_m^{II}r)B_{\upsilon,m}^{II}\right]\}\sin(\beta_m^{II}z)\exp(-i\upsilon\theta) \end{aligned} \tag{4.15}$$

$$H_z^{II} = \sum_{\upsilon=-\infty}^{\infty}\sum_{m=1}^{\infty}(k^2-(\beta_m^{II})^2)[J_\upsilon(\gamma_m^{II}r)C_{\upsilon,m}^{II} + Y_\upsilon(\gamma_m^{II}r)D_{\upsilon,m}^{II}]\times\cos(\beta_m^{II}z)\exp(-i\upsilon\theta) \quad . \tag{4.16}$$

Here, $\beta_m^{II} = m\pi / d$, is the propagation phase constant, $(\gamma_m^{II})^2 = k^2 - (\beta_m^{II})^2$ is the radial propagation constant, $m = 1, 2, 3, ...;$ $A_{\upsilon,m}^{II}, B_{\upsilon,m}^{II}, C_{\upsilon,m}^{II}, D_{\upsilon,m}^{II}$ are the undetermined coefficients.

(iii). Region *III* (i.e. $r_{w1} \le r \le r_{w2}, 180^\circ \le \theta \le 360^\circ$**)**

$$E_r^{III} = \sum_{s=1}^{\infty}\sum_{m=1}^{\infty}\left[-\beta_m^{III}\gamma_m^{III}U'_{s,m}(r)A_{s,m}^{III} + \frac{i\omega\mu s}{r}V_{s,m}(r)B_{s,m}^{III}\right]\times\cos(\beta_m^{II}\,z)\sin(s\,\theta) \tag{4.17}$$

$$E_\theta^{III} = \sum_{s=1}^{\infty}\sum_{m=1}^{\infty}\left[\frac{-s\beta_m^{III}}{r}U_{s,m}(r)A_{s,m}^{III} + i\omega\mu\gamma_m^{III}V'_{s,m}(r)B_{s,m}^{III}\right]\times\cos(\beta_m^{III}z)\cos(s\theta) \tag{4.18}$$

$$E_z^{III} = \sum_{s=1}^{\infty}\sum_{m=1}^{\infty}\left(k^2 - (\beta_m^{III})^2\right)U_{s,m}(r)A_{s,m}^{III}\times\sin(\beta_m^{III}z)\sin(s\theta) \tag{4.19}$$

$$H_r^{III} = \sum_{s=1}^{\infty}\sum_{m=1}^{\infty}\left[\frac{i\omega\varepsilon s}{r}U_{s,m}(r)A_{s,m}^{III} + \beta_m^{III}\gamma_m^{III}V'_{s,m}(r)B_{s,m}^{III}\right]\times\sin(\beta_m^{III}z)\cos(s\theta) \tag{4.20}$$

$$H_\theta^{III} = \sum_{s=1}^{\infty}\sum_{m=1}^{\infty}\left[-i\omega\varepsilon\gamma_m^{III}U'_{s,m}(r)A_{s,m}^{III} - \frac{s\beta_m^{III}}{r}V_{s,m}(r)B_{s,m}^{III}\right]\times\sin(\beta_m^{III}z)\sin(s\theta) \tag{4.21}$$

$$H_z^{III} = \sum_{s=1}^{\infty}\sum_{m=1}^{\infty}\left(k^2 - (\beta_m^{III})^2\right)V_{s,m}(r)B_{s,m}^{III}\times\cos(\beta_m^{III}z)\cos(s\theta)\ . \tag{4.22}$$

Here $\beta_m^{III} = m\pi / d,\ (\gamma_m^{III})^2 = k^2 - (\beta_m^{III})^2,\ m = 1, 2, 3...;\ s = 1, 2, 3, ...;\ A_{s,m}^{III},\ B_{s,m}^{III}$ is the undetermined coefficient; $U_{s,m},\ V_{s,m},\ U'_{s,m},\ V'_{s,m}$ represented by a Bessel function as:

$$U_{s,m}(r) = Y_s(\gamma_m^{III}r_{w2})J_s(\gamma_m^{III}r) - J_s(\gamma_m^{III}r_{w2})Y_s(\gamma_m^{III}r) \tag{4.23}$$

$$V_{s,m}(r) = Y'_s(\gamma_m^{III}r_{w2})J_s(\gamma_m^{III}r) - J'_s(\gamma_m^{III}r_{w2})\,\mathrm{Y}_s(\gamma_m^{III}r) \tag{4.24}$$

$$U'_{s,m}(r) = Y_s(\gamma_m^{III} r_{w2}) J'_s(\gamma_m^{III} r) - J_s(\gamma_m^{III} r_{w2}) Y'_s(\gamma_m^{III} r) \tag{4.25}$$

$$V'_{s,m}(r) = Y'_s(\gamma_m^{III} r_{w2}) J'_s(\gamma_m^{III} r) - J'_s(\gamma_m^{III} r_{w2}) Y'_s(\gamma_m^{III} r) \quad . \tag{4.26}$$

(iv). Boundary Conditions

(1): The boundary condition for the EM field satisfies between the region *I* and region *II* (i.e. at $r = r_d$) are:

$$E_z^I = \begin{cases} E_z^{II} & (0 \le z \le (L-T)), \quad r = r_d \\ 0 & ((L-T) \le |z| \le L), \quad r = r_c \end{cases} \tag{4.27}$$

$$E_\theta^I = \begin{cases} E_\theta^{II} & (0 \le z \le (L-T)), \quad r = r_d \\ 0 & ((L-T) \le |z| \le L), \quad r = r_c \end{cases} \tag{4.28}$$

$$H_z^I = H_z^{II} \qquad (0 \le z \le (L-T)), \tag{4.29}$$

$$H_\theta^I - H_\theta^{II} = I_z / 2\pi r_d \qquad (0 \le z \le (L-T)), \tag{4.30}$$

$$E_r^{II} - E_r^I = \rho_s / \varepsilon \qquad (0 \le z \le (L-T)), \tag{4.31}$$

here, I_z is the axial current flowing near the tip of the disc and ρ_s is the surface charge density at the interface of the discontinuity between region *I* and region *II.*

(2): The boundary condition for the EM field satisfies between the region *II* and region *III* (i.e. at $r = r_{w1}$, and $180^0 \le \theta < 360^0$) are:

$$E_z^{II} = \begin{cases} 0, & (0^\circ \le \theta \le 180^\circ), \\ E_z^{III}, & (180^\circ \le \theta \le 360^\circ), \end{cases} \tag{4.32}$$

$$E_\theta^{II} = \begin{cases} 0, & (0^\circ \le \theta \le 180^\circ), \\ E_\theta^{III}, & (180^\circ \le \theta \le 360^\circ), \end{cases} \tag{4.33}$$

$$H_z^{II} = H_z^{III} \qquad (180^\circ \le \theta \le 360^\circ), \tag{4.34}$$

$$H_\theta^{II} = H_\theta^{III} \qquad (180^\circ \le \theta \le 360^\circ), \tag{4.35}$$

Applying the boundary condition (4.27) and (4.29) we can get:

$$A_{\upsilon,n}^{I} = \sum_{\upsilon=-\infty}^{\infty}\sum_{m=1}^{\infty}\left(\frac{(k^2-(\beta_m^{II})^2)}{(k^2-(\beta_n^{I})^2)U_{\upsilon,n}(r_d)}\right)\left(\frac{S_1}{L}\right)\times\left\{J_\upsilon(\gamma_m^{II}r_d)A_{\upsilon,m}^{II}+Y_\upsilon(\gamma_m^{II}r_d)B_{\upsilon,m}^{II}\right\} \tag{4.36}$$

$$B_{\upsilon,n}^{I} = \sum_{\upsilon=-\infty}^{\infty}\sum_{m=1}^{\infty}\left(\frac{(k^2-(\beta_m^{II})^2)}{(k^2-(\beta_n^{I})^2)V_{\upsilon,n}(r_d)}\right)\left(\frac{S_2}{L-T}\right)\times\left\{J_\upsilon(\gamma_m^{II}r_d)C_{\upsilon,m}^{II}+Y_\upsilon(\gamma_m^{II}r_d)D_{\upsilon,m}^{II}\right\} \tag{4.37}$$

here, $S_1 = \int_0^{L-T} \sin(\beta_m^{II} z)e^{i\beta_n^{I} z}dz$ and, $S_2 = \int_0^{L-T} \cos(\beta_m^{II} z)e^{i\beta_n^{I} z}dz$

Similarly, applying the boundary condition (4.32) and (4.34) we can get,

$$A_{s,m}^{III} = \sum_{\upsilon=-\infty}^{\infty}\sum_{m=1}^{\infty}\left(\frac{(k^2-(\beta_m^{II})^2)S_3}{(k^2-(\beta_m^{III})^2)U_{s,m}(r_{w1})}\right)\times\left\{J_\upsilon(\gamma_m^{II}r_{w1})A_{\upsilon,m}^{II}+Y_\upsilon(\gamma_m^{II}r_{w1})B_{\upsilon,m}^{II}\right\} \tag{4.38}$$

$$B_{s,m}^{III} = \sum_{\upsilon=-\infty}^{\infty}\sum_{m=1}^{\infty}\left(\frac{(k^2-(\beta_m^{II})^2)S_4}{(k^2-(\beta_m^{III})^2)V_{s,m}(r_{w1})}\right)\times\left\{J_\upsilon(\gamma_m^{II}r_{w1})C_{\upsilon,m}^{II}+Y_\upsilon(\gamma_m^{II}r_{w1})D_{\upsilon,m}^{II}\right\} \tag{4.39}$$

here, $S_3 = \left(\frac{2}{\pi}\right)\int_{180^0}^{360^0} \sin(s\theta)e^{-i\upsilon\theta}d\theta$, and $S_4 = \left(\frac{2}{\pi}\right)\int_{180^0}^{360^0} \cos(s\theta)e^{-i\upsilon\theta}d\theta$

Now to get the coefficient of electric and magnetic field components of the region *II* (*i.e.* $A_{\upsilon,m}^{II}$, $B_{\upsilon,m}^{II}$, $C_{\upsilon,m}^{II}$, and $D_{\upsilon,m}^{II}$), applying boundary condition (4.28), (4.33), and (4.35) we get:

$$\sum_{\upsilon=-\infty}^{\infty}\sum_{m=1}^{\infty} F_{1,A}A_{\upsilon,m}^{II} + F_{1,B}B_{\upsilon,m}^{II} + F_{1,C}C_{\upsilon,m}^{II} + F_{1,D}D_{\upsilon,m}^{II} = 0 \tag{4.40}$$

$$\sum_{\upsilon=-\infty}^{\infty}\sum_{m=1}^{\infty} F_{2,A}A_{\upsilon,m}^{II} + F_{2,B}B_{\upsilon,m}^{II} + F_{2,C}C_{\upsilon,m}^{II} + F_{2,D}D_{\upsilon,m}^{II} = 0 \tag{4.41}$$

$$\sum_{\upsilon=-\infty}^{\infty}\sum_{m=1}^{\infty} F_{3,A}A_{\upsilon,m}^{II} + F_{3,B}B_{\upsilon,m}^{II} + F_{3,C}C_{\upsilon,m}^{II} + F_{3,D}D_{\upsilon,m}^{II} = 0 \tag{4.42}$$

where,

$$F_{1,A} = \left\{\frac{i\upsilon\beta_m^{II}}{r_d} - \sum_{n=-\infty}^{\infty}\frac{\upsilon\beta_n^{I}(k^2-(\beta_m^{II})^2)}{r_d(k^2-(\beta_n^{I})^2)}\right\}\times J_\upsilon(\gamma_m^{II}r_d)\times\left(\frac{S_1}{L}\right)$$

$$F_{1,B} = \left\{\frac{i\upsilon\beta_m^{II}}{r_d} - \sum_{n=-\infty}^{\infty}\frac{\upsilon\beta_n^{I}(k^2-(\beta_m^{II})^2)}{r_d(k^2-(\beta_n^{I})^2)}\right\}\times Y_\upsilon(\gamma_m^{II}r_d)\times\left(\frac{S_1}{L}\right)$$

$$F_{1,C} = \{i\omega\upsilon\gamma_m^{II}J_\upsilon'(\gamma_m^{II}r_d)S_2/(L-T)\} - \sum_{n=-\infty}^{\infty}\frac{i\omega\upsilon\gamma_n^{I}(k^2-(\beta_m^{II})^2)J_\upsilon(\gamma_m^{II}r_d)V_{\upsilon,n}'(r_d)S_2}{(k^2-(\beta_n^{I})^2)V_{\upsilon,n}(r_d)(L-T)}$$

$$F_{1,D} = \{i\omega\upsilon\gamma_m^{II}Y_\upsilon'(\gamma_m^{II}r_d)S_2/(L-T)\} - \sum_{n=-\infty}^{\infty}\frac{i\omega\upsilon\gamma_n^{I}(k^2-(\beta_m^{II})^2)Y_\upsilon(\gamma_m^{II}r_d)V_{\upsilon,n}'(r_d)S_2}{(k^2-(\beta_n^{I})^2)V_{\upsilon,n}(r_d)(L-T)}$$

$$F_{2,A} = \frac{i\upsilon\beta_m^{II}}{r_{w1}}J_\upsilon(\gamma_m^{II}r_{w1})S_3 + \sum_{s=1}^{\infty}\frac{s\beta_m^{III}(k^2-(\beta_m^{II})^2)J_\upsilon(\gamma_m^{II}r_{w1})}{r_{w1}(k^2-(\beta_m^{III})^2)}S_3^2$$

$$F_{2,B} = \frac{i\upsilon\beta_m^{II}}{r_{w1}} Y_\upsilon(\gamma_m^{II} r_{w1}) S_3 + \sum_{s=1}^{\infty} \frac{s\beta_m^{III}(k^2 - (\beta_m^{II})^2) Y_\upsilon(\gamma_m^{II} r_{w1})}{r_{w1}(k^2 - (\beta_m^{III})^2)} S_3^2$$

$$F_{2,C} = i\omega\mu\gamma_m^{II} J'_\upsilon(\gamma_m^{II} r_{w1}) S_3 - \sum_{s=1}^{\infty} \frac{i\omega\mu\gamma_m^{III} V'_{s,m}(r_{w1})(k^2 - (\beta_m^{II})^2) J_\upsilon(\gamma_m^{II} r_{w1})}{(k^2 - (\beta_m^{III})^2) V_{s,m}(r_{w1})} S_3 S_4$$

$$F_{2,D} = i\omega\mu\gamma_m^{II} Y'_\upsilon(\gamma_m^{II} r_{w1}) S_3 - \sum_{s=1}^{\infty} \frac{i\omega\mu\gamma_m^{III} V'_{s,m}(r_{w1})(k^2 - (\beta_m^{II})^2) Y_\upsilon(\gamma_m^{II} r_{w1})}{(k^2 - (\beta_m^{III})^2) V_{s,m}(r_{w1})} S_3 S_4$$

$$F_{3,A} = -i\omega\varepsilon\gamma_m^{II} J'_\upsilon(\gamma_m^{II} r_{w1}) S_4 + \sum_{s=1}^{\infty} \frac{i\omega\varepsilon\gamma_m^{III} U'_{s,m}(r_{w1})(k^2 - (\beta_m^{II})^2) J_\upsilon(\gamma_m^{II} r_{w1})}{(k^2 - (\beta_m^{III})^2) U_{s,m}(r_{w1})} S_3 S_4$$

$$F_{3,B} = -i\omega\varepsilon\gamma_m^{II} Y'_\upsilon(\gamma_m^{II} r_{w1}) S_4 + \sum_{s=1}^{\infty} \frac{i\omega\varepsilon\gamma_m^{III} U'_{s,m}(r_{w1})(k^2 - (\beta_m^{II})^2) Y_\upsilon(\gamma_m^{II} r_{w1})}{(k^2 - (\beta_m^{III})^2) U_{s,m}(r_{w1})} S_3 S_4$$

$$F_{3,C} = -\frac{i\upsilon\beta_m^{II}}{r_{w1}} J_\upsilon(\gamma_m^{II} r_{w1}) S_4 + \sum_{s=1}^{\infty} \frac{s\beta_m^{III}(k^2 - (\beta_m^{II})^2) J_\upsilon(\gamma_m^{II} r_{w1})}{r_{w1}(k^2 - (\beta_m^{III})^2)} S_4^2$$

$$F_{3,D} = -\frac{i\upsilon\beta_m^{II}}{r_{w1}} Y_\upsilon(\gamma_m^{II} r_{w1}) S_4 + \sum_{s=1}^{\infty} \frac{s\beta_m^{III}(k^2 - (\beta_m^{II})^2) Y_\upsilon(\gamma_m^{II} r_{w1})}{r_{w1}(k^2 - (\beta_m^{III})^2)} S_4^2$$

Using Eqs. (4.40), (4.41) and (4.42), $B_{\upsilon,m}^{II}$, $C_{\upsilon,m}^{II}$ and $D_{\upsilon,m}^{II}$ can be represented in the term of $A_{\upsilon,m}^{II}$ as:

$$B_{\upsilon,m}^{II} = G_{B,A} A_{\upsilon,m}^{II} \tag{4.43}$$

$$C_{\upsilon,m}^{II} = G_{C,A} A_{\upsilon,m}^{II} \tag{4.44}$$

$$D_{\upsilon,m}^{II} = G_{D,A} A_{\upsilon,m}^{II} \tag{4.45}$$

here,

$$G_{B,A} = -\frac{(F_{1,A}F_{2,C} - F_{2,A}F_{1,C})(F_{2,C}F_{3,D} - F_{2,D}F_{3,C}) + (F_{1,D}F_{2,C} - F_{2,D}F_{1,C})(F_{3,C}F_{2,A} - F_{2,C}F_{3,A})}{(F_{1,B}F_{2,C} - F_{2,B}F_{1,C})(F_{2,C}F_{3,D} - F_{2,D}F_{3,C}) + (F_{1,D}F_{2,C} - F_{2,D}F_{1,C})(F_{3,C}F_{2,B} - F_{2,C}F_{3,B})}$$

$$G_{C,A} = -\frac{(F_{1,A}F_{2,B} - F_{2,A}F_{1,B})(F_{2,B}F_{3,D} - F_{2,D}F_{3,B}) + (F_{1,D}F_{2,B} - F_{2,D}F_{1,B})(F_{3,B}F_{2,A} - F_{2,B}F_{3,A})}{(F_{1,C}F_{2,B} - F_{2,C}F_{1,B})(F_{2,B}F_{3,D} - F_{2,D}F_{3,B}) + (F_{1,D}F_{2,B} - F_{2,D}F_{1,B})(F_{3,B}F_{2,C} - F_{3,C}F_{2,B})}$$

$$G_{D,A} = -\frac{(F_{1,A}F_{2,B} - F_{2,A}F_{1,B})(F_{2,B}F_{3,C} - F_{2,C}F_{3,B}) + (F_{1,C}F_{2,B} - F_{2,C}F_{1,B})(F_{3,B}F_{2,A} - F_{2,B}F_{3,A})}{(F_{1,C}F_{2,B} - F_{2,C}F_{1,B})(F_{2,D}F_{3,B} - F_{2,B}F_{3,D}) + (F_{1,D}F_{2,B} - F_{2,D}F_{1,B})(F_{3,C}F_{2,B} - F_{3,B}F_{2,C})}$$

Using Eqs. (4.36) and (4.43) $A_{\upsilon,m}^{II}$ can be represented in terms of $A_{\upsilon,n}^{I}$ as:

$$A_{\upsilon,m}^{II} = \sum_{n=-\infty}^{\infty} M_{n,m} A_{\upsilon,n}^{I} \tag{4.46}$$

where, $M_{n,m} = \frac{(k^2 - (\beta_n^I)^2) U_{\upsilon,n}(r_d)}{(k^2 - (\beta_m^{II})^2)\{J_\upsilon(\gamma_m^{II} r_d) + G_{B,A} Y_\upsilon(\gamma_m^{II} r_d)\}} \left(\frac{\bar{S}_1}{L}\right)$

4.3.1. Equivalent shunt Capacitance per unit length

The equivalent shunt capacitance per unit length for the azimuthally partitioned axially periodic metal disc loaded coaxial structure can be obtained using the current telegraphist's equation of the structure equivalent transmission line. The current telegraphist's equation relates the circuit potential to the axial current of the disc-loaded structure and form equivalent shunt capacitance per unit length [Dixit and Jain (2016)]:

$$C_e = \frac{\beta_n}{\omega} \frac{I_z}{V}. \tag{4.47}$$

To find the axial current-voltage ratio (I_z / V), the electric field constant of the region *I* ($A_{\upsilon,n}^{I}$) is expressed in terms of I_z using the boundary condition (4.30). Further,

$\sin(\beta_m^{II} z)$ is multiplied both sides in Eq. (4.30) and after integration from limit ($0 \le z < (L-T)$), we get,

$$\int_0^{L-T} (H_\theta^{II} - H_\theta^{I}) \sin(\beta_m^{II} z) dz = \int_0^{L-T} \frac{I_z}{2\pi r_d} \sin(\beta_m^{II} z) dz . \tag{4.48}$$

Substituting Eqs. (4.5) and (4.15) in the above equation, one can express I_z in terms of electric and magnetic constants ($A_{\upsilon,m}^{II}, B_{\upsilon,m}^{II}$, $C_{\upsilon,m}^{II}$ and $D_{\upsilon,m}^{II}$) of region *II*. Further, substituting region *II* field constants in terms of the region *I* electric field constant ($A_{\upsilon,n}^{I}$) using Eqs. (4.43)-(4.46) and after rearranging, we get,

$$A_{\upsilon,n}^{I} = R_{\upsilon,nm} I_z . \tag{4.49}$$

where $R_{\upsilon,nm}$ is defined as,

$$R_{\upsilon,nm} = \sum_{m=1}^{\infty} [i\omega\varepsilon \gamma_n^I U'_{\upsilon,n}(r_d) - \frac{i\omega\varepsilon(L-T)\gamma_m^{II} M_{n,m}}{2} \{J'_\upsilon(\gamma_m^{II} r_d) + G_{B,A} Y'_\upsilon(\gamma_m^{II} r_d)\}$$
$$- \frac{i\upsilon M_{n,m} (J_\upsilon(\gamma_m^{II} r_d) G_{C,A} + Y_\upsilon(\gamma_m^{II} r_d) G_{D,A})}{r_d} \{\frac{\beta_m^{II}(L-T)}{2} - \frac{i\beta_n^I (k^2 - (\beta_m^{II})^2)\bar{S}_1}{2(k^2 - (\beta_n^I)^2)}\}]^{-1}$$

At the boundary of the region *I* and region *II*, axial electric field (E_z^I) is expressed in terms of axial current (I_z) using Eqs. (4.3) and (4.49), written as,

$$E_z^I = \sum_{\upsilon=-\infty}^{\infty} \sum_{n=-\infty}^{\infty} P_{\upsilon,nm} I_z \tag{4.50}$$

with, $$P_{\upsilon,nm} = \sum_{n=-\infty}^{\infty} \frac{R_{\upsilon,nm}(k^2 - (\beta_n^I)^2) U_{\upsilon,n}(r_d) \bar{S}_1}{2\pi r_d}$$

Now, the electric field (E_z^I) can be express in terms of scalar potential *V* as [Dixit and Jain (2016)]:

$$E_z^I = j\left(\frac{(\gamma_n^I)^2}{\beta_n^I}\right)V \quad . \tag{4.51}$$

Using Eqs. (4.50) and (4.51), we can find the ratio of the axial current and voltage and after substituting this ratio in Eq. (4.47) the equivalent shunt capacitance per unit length (C_e) in terms of structure parameter for different azimuthal mode number can be obtained as:

$$(C_e)_\upsilon = \frac{j(\gamma_n^I)^2}{\omega}\frac{1}{P_{\upsilon,nm}} . \tag{4.52}$$

4.3.2. Equivalent series inductance per unit length

The equivalent series inductance per unit length for the azimuthally partitioned axially periodic metal disc loaded coaxial structure can be obtained using voltage telegraphist's equation, given as [Dixit and Jain (2016)],

$$L_e = \left(\frac{\beta_n}{\omega}\right)\frac{V}{I_\theta} . \tag{4.53}$$

Here, voltage to the current ratio (V / I_θ) obtained using the boundary condition (4.31) with the multiplication of $\sin(\beta_m^{II} z)$ and integration from limit ($0 \le z < (L-T)$) similar to that of Eq. (4.48), we get,

$$\int_0^{L-T} (E_r^{II} - E_r^I)\sin(\beta_m^{II} z)dz = \int_0^{L-T} \frac{\rho_s}{\varepsilon}\sin(\beta_m^{II} z)dz = \int_0^{L-T} \frac{I_\theta}{2\pi r_d \varepsilon}\sin(\beta_m^{II} z)dz \ . \tag{4.54}$$

Now, substituting Eqs. (4.1) and (4.11) in the above equation and after simplification, we can get I_θ in terms of electric and magnetic field constants ($A_{\upsilon,m}^{II}, B_{\upsilon,m}^{II}, C_{\upsilon,m}^{II}$, and $D_{\upsilon,m}^{II}$) of region *II*. Further, using Eqs. (4.43)-(4.46) and after rearranging, we can get, region *II* field constants in terms of the region *I* electric field constant ($A_{\upsilon,n}^{I}$) as:

$$A_{\upsilon,n}^{I} = Q_{\upsilon,nm} I_\theta \tag{4.55}$$

$$Q_{\upsilon,nm} = \sum_{m=1}^{\infty} [i\beta_n^I \gamma_n^I U_{\upsilon,n}(r_d) - \frac{\upsilon\omega\mu(k^2 - (\beta_m^{II})^2) S_2 \left(J_\upsilon(\gamma_m^{II} r_d) G_{C,A} + Y_\upsilon(\gamma_m^{II} r_d) G_{D,A} \right)}{r_d (L-T)(k^2 - (\beta_n^I)^2)}]^{-1}.$$

Now, the axial electric field (E_z^I) is expressed in terms of current (I_θ) using Eqs. (4.3) and (4.55), written as,

$$E_z^I = \sum_{\upsilon=-\infty}^{\infty} \sum_{n=-\infty}^{\infty} W_{\upsilon,nm} I_\theta, \tag{4.56}$$

where, $W_{\upsilon,nm} = \sum_{n=-\infty}^{\infty} \frac{Q_{\upsilon,nm} U_{\upsilon,n}(r_d) \bar{S}_1}{2\pi r_d}$.

Now, similar to the equivalent shunt capacitance per unit length (C_e), equivalent series inductance per unit length (L_e) can be obtained the ratio of the voltage and current (V / I_θ) Eqs. (4.51) and (4.56). After substituting this ratio in Eqs. (4.53) the equivalent series inductance per unit length (L_e) for different azimuthal mode number can be obtained in terms of structure parameter written as,

$$(L_e)_\upsilon = \frac{1}{j\omega} \left(\frac{\beta_n^I}{\gamma_n^I} \right)^2 \times \frac{1}{W_{\upsilon,nm}}. \tag{4.57}$$

4.3.3. Phase Velocity of different modes

To reduce the phase velocity of the desired modes below than speed of light so that it can be synchronized with the electron beam velocity, an azimuthally partitioned axially periodic metal disc loaded coaxial structure can be used. With the consideration of equivalent shunt capacitance per unit length for different modes ($(C_e)_\upsilon$) and equivalent series inductance per unit length for different modes ($(L_e)_\upsilon$), the phase velocity of the structure for different modes can be calculated using the popular well-known relationship:

$$(v_p)_\upsilon = 1/((L_e)_\upsilon (C_e)_\upsilon)^{1/2}. \tag{4.58}$$

4.3.4. Dispersion Relation

The EM wave propagation behavior of the azimuthally partitioned axially periodic metal disc loaded coaxial structure can easily be described with the help of its dispersion relation. The dispersion relation of this structure for different modes in terms of structure parameters, the equivalent shunt capacitance per unit length for different modes ($(C_e)_\upsilon$) and equivalent series inductance per unit length for different modes ($(L_e)_\upsilon$) developed in the previous section used in the equation can be given as [Dixit and Jain (2016)]:

$$\beta^2 - \omega^2 (L_e)_\upsilon (C_e)_\upsilon = 0 \quad . \tag{4.59}$$

After rearranging the above equation, we get a similar expression as derived through the involved and cumbersome field analysis [Wang *et al.* (2010)].

4.3.5. Characteristic impedance of different modes

The characteristic impedance of the structure which is important from the impedance matching consideration for different operating modes of the azimuthally partitioned axially periodic metal disc loaded coaxial structure can be obtained using the relationship given as [Dixit and Jain (2016)]:

$$(Z_0)_\upsilon = ((L_e)_\upsilon / (C_e)_\upsilon)^{1/2}. \tag{4.60}$$

4.4. Results and Discussion

The azimuthally partitioned axially periodic metal disc loaded coaxial structure is used as an RF interaction structure in MILO for temporal growth of two stable and separate frequencies within a single device. A dispersion relation is an excellent tool that provides information about the resonant frequency of the interaction structure and highlights the effect of various structural parameters on the phase-shift variation with frequency. Since the resonating frequency of any structure depends upon the structural dimension (i.e. mainly inner radius of the cavity), therefore the characteristics of azimuthally uniform and azimuthally partitioned axially periodic metal disc loaded coaxial structures is compared (i.e. the dispersion curves are numerically calculated). The dispersion curve helps in calculating the phase velocity and group velocity of the associated modes, which further helps in estimating the possibility of the corresponding mode to oscillate. The dispersion relation for the fundamental mode (i.e. TM_{00} mode) is calculated for azimuthally uniform structure using Eqs. (4.59) with considering υ=0 to observe the effect of the cavity wall radius, which is shown in Fig. 4.2. From this figure, we can observe that the beam-line intersects the dispersion curve at two points,

which represents the operating frequencies of two different azimuthally uniform structures (i.e. structure-1 with the wall radius r_w=140 mm (red color) and structure-2 with the wall radius of r_w =129 mm (green color) considering) while the other design parameters are unchanged. To combine the effect of two different wall radii in a single device, the dispersion curve for the azimuthally partitioned structure is shown in Fig. 4.3. The dispersion relation derived in Eqs. (4.59) is used to obtain the dispersion curve for different modes by considering υ=0 for Mode-A and υ=1 for Mode-B. From Fig. 4.3, it can be observed that for two different modes, the beams line intersects at two points on the dispersion curve which indicates that the different synchronizing frequencies exist within this single structure. Here, one frequency associated with one part of the azimuthal section (i.e. r_{w1} =140 mm and azimuthal range 180^0-360^0 (blue color) which is considered as Mode-A) and another one is associated with the other part of the azimuthal section (i.e. r_{w2} =129 mm and azimuthal range 0^0-180^0 (brown color) which is considered as Mode-B). Due to the absence of the azimuthal symmetry in the structure, the symmetric TM or TE mode does not exist independently [Wang *et al.* (2010)]. For the appropriate electron beam and RF wave interaction, the essential condition for any mode is that the group velocity of the corresponding mode should be close to zero. The normalized group and phase velocity associated with the different modes i.e. for the azimuthally uniform structure and azimuthally partitioned structure is shown in Fig. 4.4. Fig. 4.4(a) shows the normalized group velocity of the fundamental mode associated with an azimuthally uniform structure and azimuthally partitioned structure. After finding the propagation constant value limit for beam wave synchronized operation, the phase velocities associated with the different modes are calculated. The point where the RF phase velocity of the specific mode and drift

velocity of the electrons intersects is considered as the operating point of that corresponding mode. Fig. 4.4(b) shows the normalized phase velocity associated with the different modes due to the azimuthally uniform structure and azimuthally partitioned structure. It can be seen from Fig. 4.4(b) that, the phase velocity of Mode-A equals to the phase velocity of an azimuthal uniform structure having an outer cavity radius of 140 mm, and the phase velocity of Mode-B, matches with the phase velocity of an azimuthal uniform structure having outer cavity radius 129 mm.

Since MILO is a coaxial cross-field (M-type) device in which electrons are emitted from the cathode drifts along the axial direction (i.e. $\hat{v}_z = \hat{E} \times \hat{B}$) under the action of the orthogonal radial electric field and the angular magnetic field and interacts with the eigenmode of the RF interaction structure resulting temporal growth of the microwave field. Because the electrons move in the axial direction, the electrons involved in the beam-wave interactions at different regions in the angular direction (i.e. 0^0-180^0 and 180^0-360^0) are relatively independent processes. Therefore, through the azimuthally partitioned structure which is used in BFMILO, Mode-A and Mode-B will oscillate independently. Furthermore, the effect of the cavity's wall radius on the frequency difference between two operating frequencies (i.e. between the Mode-A and Mode-B) is shown in Fig. 4.5. From this figure, it can be easily concluded that the frequency difference mainly depends upon the cavity wall radius (i.e. r_w).

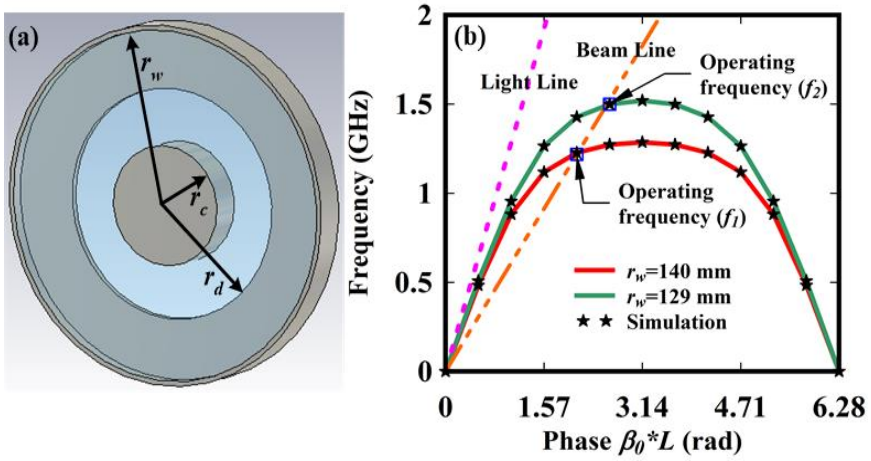

Figure 4.2: Unit cell structure and corresponding dispersion curve for azimuthally uniform disc-loaded coaxial structure with different wall radii (r_w) of 129 mm, and 140 mm (r_c=53 mm, r_d=86 mm, L=27 mm, and T=5 mm).

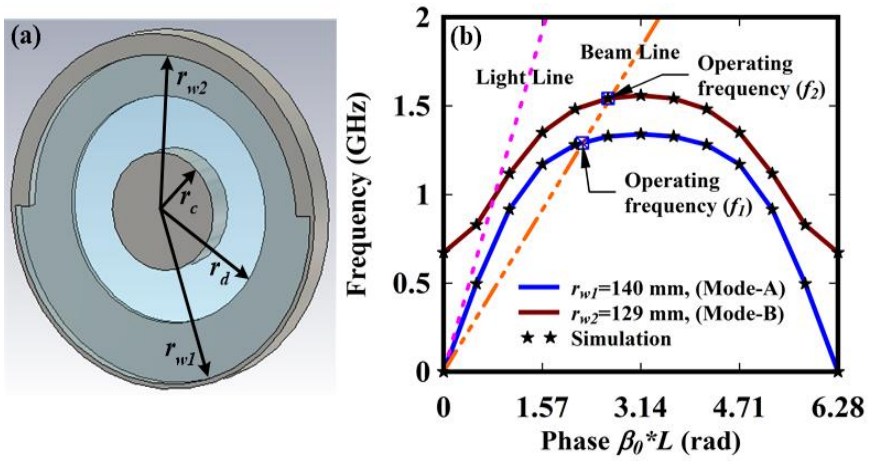

Figure 4.3: Unit cell structure and corresponding dispersion curve for azimuthally partitioned disc-loaded coaxial structure with different wall radii r_{w1}= 140 mm, and r_{w2}=129 mm (with, r_c=53 mm, r_d=86 mm, L=27 mm, and T=5 mm).

By varying the cavity's wall radius r_w, the phase shift associated with the mode is limited by the phase velocity of that corresponding mode which should belong to the region of operation. The maximum frequency shift of 600 MHz in L-band is attained by

the typical structure (taken in the present chapter) by changing only cavity wall radius (r_w) keeping other design parameters unchanged.

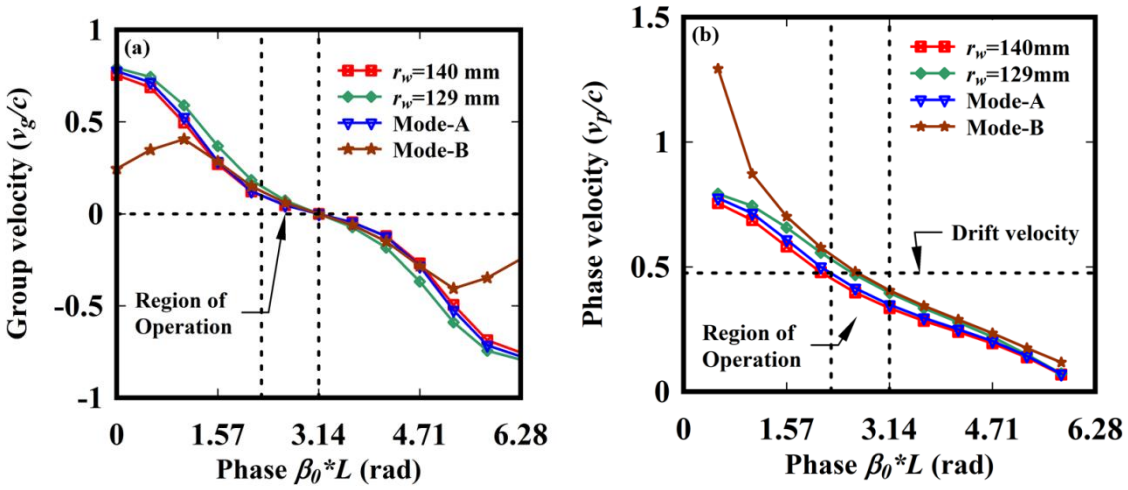

Figure 4.4: Normalized group velocity and phase velocity of the azimuthally uniform and azimuthally partitioned coaxial structure: (a) normalized group velocity, and (b) normalized phase velocity.

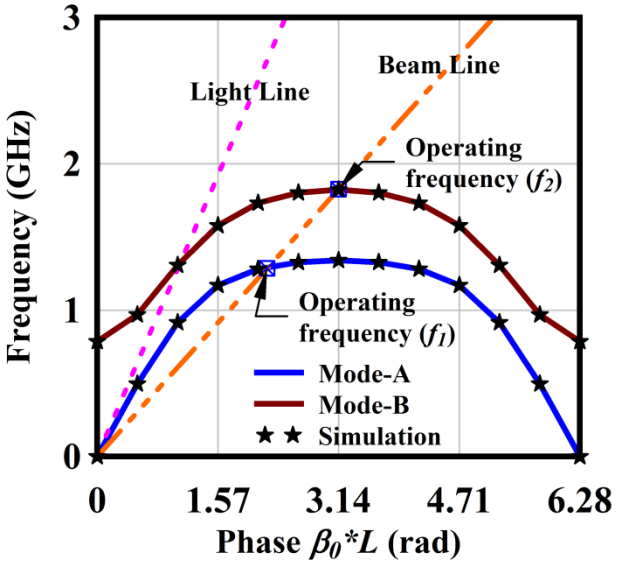

Figure 4.5: Frequency range shift attained through the azimuthally partitioned coaxial structure by changing wall radius (r_w).

The equivalent shunt capacitance and series inductance per unit length of the equivalent transmission line for the two modes associated with the azimuthal uniform (i.e. with different wall radii) and azimuthally partitioned structure are numerically calculated and shown in Fig. 4.6. The shunt capacitance per unit length is shown in Fig. 4.6(a) and It can be seen from the figure that the shunt capacitance per unit length for two resonating modes of azimuthally partitioned structure matches with the corresponding azimuthally uniform structure fundamental modes (i.e. $r_w = 140\,\text{mm}$ matches with Mode-A and $r_w = 129\,\text{mm}$ matches with Mode-B). A similar effect is also observed for the series inductance per unit length which is shown in Fig. 4.6(b).

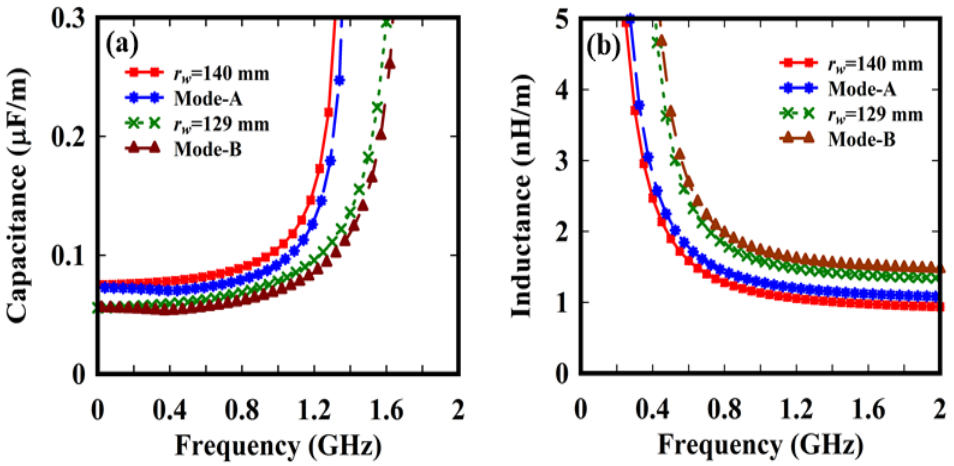

Figure 4.6: Equivalent shunt capacitance and equivalent series inductance of the transmission line: (a) Shunt capacitance per unit length (b) Series inductance per unit length of the equivalent transmission line for azimuthal uniform (r_w=140 mm and 129 mm) and azimuthal partitioned disc-loaded coaxial structure (with r_{w1}=140 mm, r_{w2}=129 mm).

To identify the different modes associated with the azimuthally partitioned axially periodic disc-loaded coaxial structure, the electric and magnetic fields

distribution vector is shown in Figs. 4.7 and 4.8, respectively. It can be seen from Figs. 4.7 and 4.8, the vector field associated with Mode-A (i.e. $180^{\circ} \le \theta \le 360^{\circ}$) and Mode-B (i.e. $0^{\circ} \le \theta \le 180^{\circ}$) confirms the operating frequencies of the structure. With the vector field distribution, we can observe that for Mode-A, the electric field and magnetic field distribution is mainly concentrated in one half of the azimuthal region (i.e. $180^{\circ} \le \theta \le 360^{\circ}$) and does not show the characteristic of perfect TE or TM mode (thus considered as a hybrid mode).

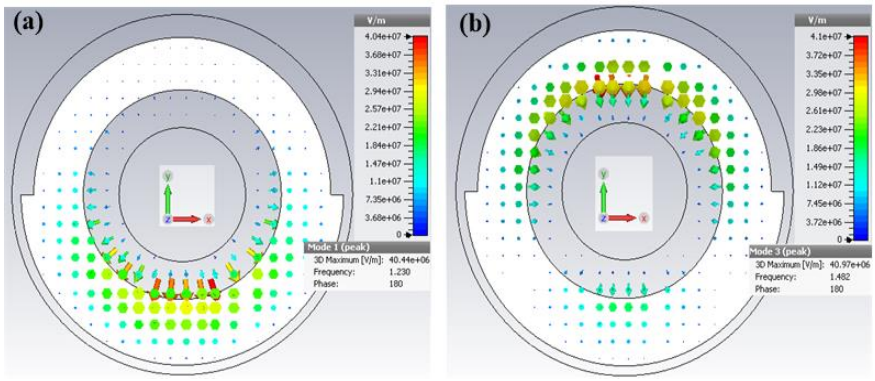

Figure 4.7: Electric field distribution vector of the azimuthal partitioned coaxial structure (a) for Mode-A and, (b) for Mode-B.

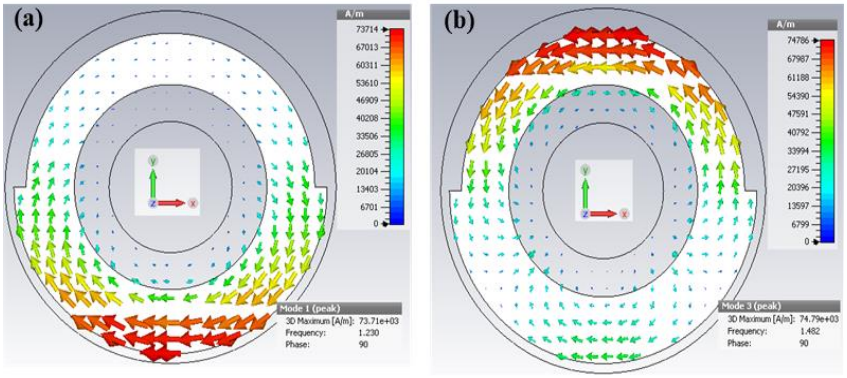

Figure 4.8: Magnetic field distribution vector of the azimuthally partitioned structure (a) for Mode-A and, (b) for Mode-B.

Similarly, for Mode-B, the electric and magnetic fields distribution are mainly concentrated in another half of the azimuthal region ($0^\circ \le \theta \le 180^\circ$).

To further verify the bi-frequency generation by the azimuthally partitioned structure, a finite length structure with two cavity depth at $0^\circ \le \theta \le 180^\circ$ and $180^\circ \le \theta \le 360^\circ$ shown in Fig. 4.9(a) is considering for the cold characterization (in absence of the electron beam). The beam absent EM simulation of the structure is performed using a well-accepted commercial tool 'CST Studio Suite'. The normalized power distribution inside the structure is shown in Fig. 4.9(b). It can be observed from the figure that the power is distributed mainly in these two frequencies which validate the potential of bi-frequency generation with the azimuthally partitioned axially periodic disc-loaded coaxial structure.

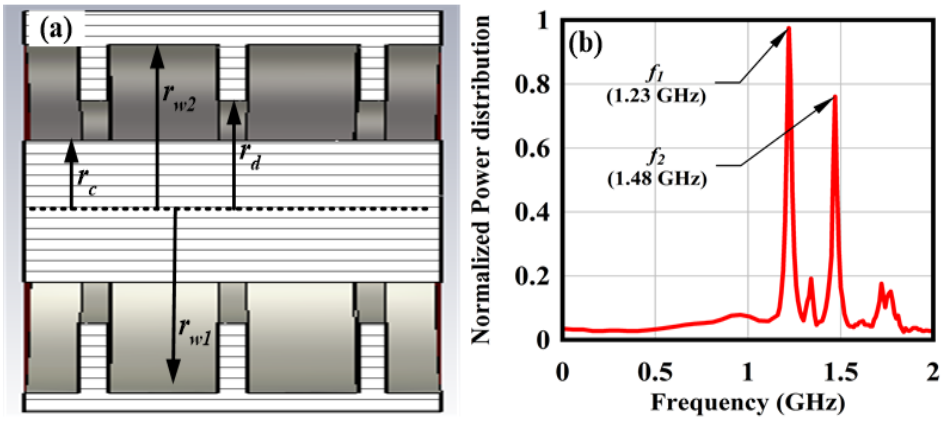

Figure 4.9: (a) Schematic (b) Normalized power distribution versus frequency response of a typical azimuthally partitioned axially periodic disc loaded coaxial structure.

4.4.1 Effect of variation of structure parameters

The effect of structure parameter variation on the dispersion characteristics for

two different modes associated with the azimuthal partitioned axially periodic disc loaded coaxial structure is shown in Fig. 4.10. Fig. 4.10(a), 4.10(b), 4.10(c), and 4.10(d)

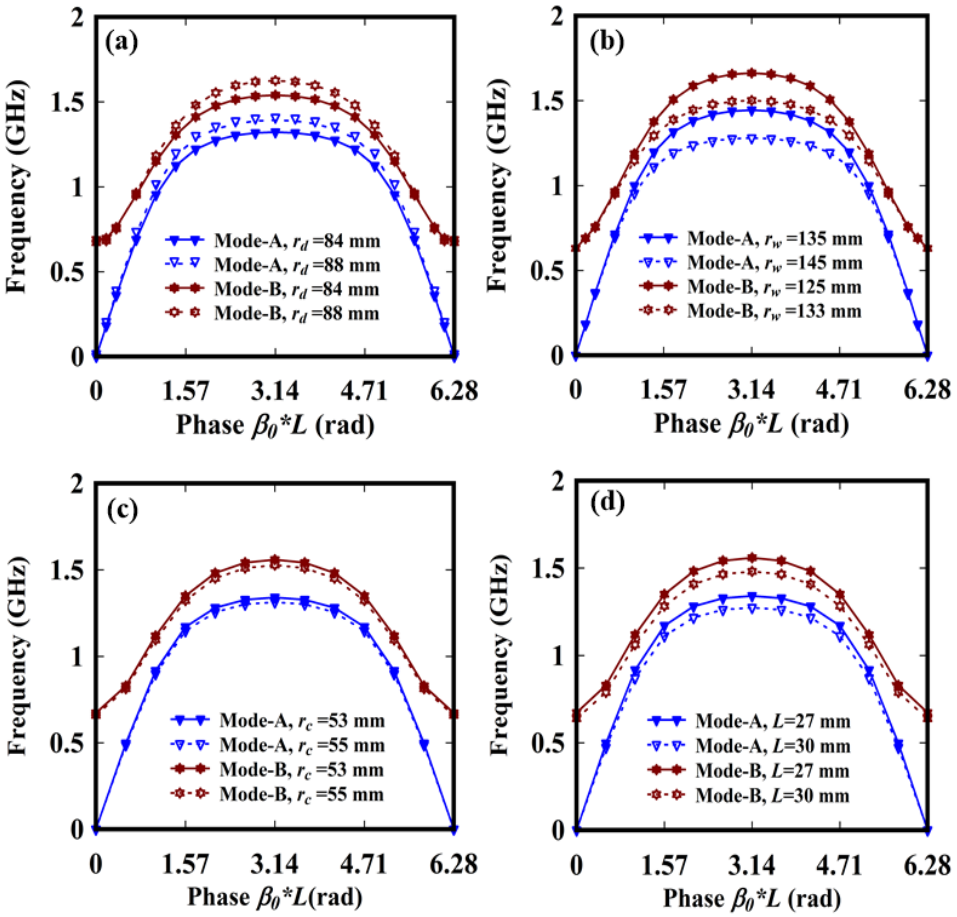

Figure 4.10: Effect of different structural parameters on the dispersion behavior of the azimuthally partitioned axially periodic disc loaded coaxial structure: (a) disc inner radius (r_d), (b) waveguide wall radius (r_w), (c) cathode radius (r_c), and (d) disc periodicity (L).

depict the sensitivity of the variation of disc inner radius (r_d), cavity wall radius (r_w), cathode radius (r_c), and disc periodicity (L) on the operating modes of the azimuthal partitioned axially periodic disc loaded coaxial structure, respectively. Fig. 4.10(a) shows that with the increase in disc inner radius (r_d), the dispersion curve gets shifted in

an upward direction, indicating an increase in the frequency with the corresponding mode. Fig. 4.10(b) shows that with the increase in the cavity waveguide wall radius r_w, the dispersion curve shifted in a downward direction which indicates that the frequency associated with both modes decreases. Fig. 4.10(c) shows the effect of the cathode radius on the dispersion curve; here it can be observed that variation in the cathode radius does not cause much effect on structure dispersion. Fig. 4.10(d) shows the effect of disc periodicity (L) on the dispersion curve and observed that with the increase in periodicity, the dispersion curve shifted downward indicating a decrease in the structure operating frequency associated with the different modes.

4.5. Conclusion

In this chapter, we have considered an azimuthally partitioned axially periodic metal disc loaded coaxial structure, which can be used as the MILO RF interaction structure for the bi-frequency HPM generation. This structure is analyzed using the equivalent circuit approach which is found much simpler, less cumbersome, and yields equally accurate results that the more involved and rigorous field analytical approach. Considering the azimuthally portioned metal RF interaction structure as loss-free, expressions for the equivalent series inductance per unit length and equivalent capacitance per unit length of its equivalent transmission line are obtained. These series inductance and shunt capacitance expressions are used for deriving the structure dispersion relation, phase velocity, and as well as characteristic impedance. Since the structure is azimuthally asymmetric, the symmetric TE and TM modes do not exist independently and the two modes excited in the azimuthally partitioned structure are studied. To confirm the structure capable of supporting bi-frequency; the dispersion

behavior of the azimuthally uniform structure of different wall radius is studied through the developed analysis and simulation. To find the structure operation region and the frequency bandwidth possible between the modes, the group and phase velocities are analytically computed. EM fields excited in the azimuthally partitioned structure are simulated which confirms the excitation of two modes as predicted by the present analysis. The parametric study is also made to analyze the crucial structural parameters which affect the operating frequency associated with the excited modes in the azimuthally partitioned structure. The dispersion values obtained by the developed analysis and simulation results are found within 5%.